SCIENCE CHINA Materials ARTICLES

mater.scichina.com link.springer.com

Published online 9 September 2020 | https://doi.org/10.1007/s40843-020-1458-5
Sci China Mater 2021, 64(3): 651–663

Non-noble metal single-atom catalyst of Co_1/MXene (Mo_2CS_2) for CO oxidation

Shamraiz Hussain Talib[1], Sambath Baskaran[2], Xiaohu Yu[3*], Qi Yu[3], Beenish Bashir[1], Shabbir Muhammad[4], Sajjad Hussain[5], Xuenian Chen[5] and Jun Li[1,2*]

ABSTRACT MXene is a variety of new two-dimensional (2D) materials with early transition metal carbides, nitrides, and carbonitrides. Quantum chemical studies have been carried out on the geometries, electronic structures, stability and catalytic properties of a non-noble metal single-atom catalyst (SAC) with single Co atom anchored on MXene materials of Mo_2CS_2. The Co adatom anchored on top of the Mo atom of this MXene is found to be rather stable, and this SAC is appropriate for CO oxidation. The charge transfers from the surface to the adsorbed CO and O_2 play a significant role in the activation of these molecules on Co_1/Mo_2CS_2. With this catalyst, the Eley-Rideal (ER), Langmuir-Hinshelwood (LH), and Termolecular Eley-Rideal (TER) mechanisms are explored for CO oxidation. We find that, while all the three mechanisms are feasible at low temperature, Co_1/Mo_2CS_2 possesses higher catalytic activity for CO oxidation through the TER mechanism that features an intriguing OC(OO)CO intermediate (IM) adsorbed on Co single atom. The calculated activation energy barriers of the rate-limiting step are 0.67 eV (TER), 0.78 eV (LH) and 0.88 eV (ER), respectively. The present study illustrates that it is promising to develop and design low-cost, non-noble metal SACs using MXene types of 2D materials.

Keywords: heterogeneous catalysis, 2D MXene monolayer, CO oxidation, DFT calculations, Co_1/Mo_2CS_2 single-atom catalyst

INTRODUCTION

The CO oxidation at low temperature has been one of the archetypal reactions in heterogeneous catalysis due to its importance in environmental catalysis, fuel cell applications, combustion, and other industrial processes [1–5]. Hence, CO oxidation reaction serves as a benchmark for the scrutiny of catalytic activity of heterogeneous catalysts. Noble metal catalysts such as Pt, Pd, Au, Rh [6–14], reveal promising catalytic activity for CO oxidation even in the presence of moisture [15]. However, these noble-metal catalysts are expensive, which is detrimental for their economical applications in industry. Thus, practical applications at large-scale require low-cost catalysts with high activity. Plentiful efforts have been made, including utilization of non-noble metals and reducing the size of metal catalysts [15–18]. Sub-nanosized metal clusters and nanoparticles usually possess higher catalytic activity and selectivity as compared with bulk metal [19–22]. As an effective approach to lower the cost and consumption of catalysts, single-atom catalysts (SACs), which was first proposed in 2011 [23–26], have become promising alternative in heterogeneous catalysis [27–30]. SACs embedded on different supports have revealed superb catalytic activity and selectivity as compared with sub-nanosized metal clusters [31,32]. In recent years, much attention has been given to the synthesis of nanoparticles, sub-nanometer clusters, and single atoms dispersed on the high surface area to increase the atomic efficiency of metals and to achieve the estimated catalytic conversions [33–35]. Therefore, the SACs supported on different substrates have obtained special attention because of high

[1] Department of Chemistry and Key Laboratory of Organic Optoelectronics & Molecular Engineering of Ministry of Education, Tsinghua University, Beijing 100084, China
[2] Department of Chemistry, Southern University of Science and Technology, Shenzhen 518055, China
[3] Shaanxi Key Laboratory of Catalysis, Shaanxi University of Technology, Hanzhong 723000, China
[4] Research Center for Advanced Materials Sciences (RCAMS), King Khalid University, Abha 61413, P.O. Box 9004, Saudi Arabia
[5] School of Chemistry and Chemical Engineering, Henan Key Laboratory of Boron Chemistry and Advanced Energy Materials, Henan Normal University, Xinxiang 453007, China
* Corresponding authors (emails: junli@tsinghua.edu.cn (Li J); yuxiaohu@snut.edu.cn (Yu X))

catalytic activity, selectivity, efficiency and low cost [36]. For example, Zhang's group [23] for the first time experimentally prepared and verified Pt single atoms dispersed on the surface of iron oxide for CO oxidation reaction with high stability, high activity and excellent catalytic performance. In another article, Nie *et al.* [37] reported that atomically dispersed Pt single atoms embedded on the CeO_2 surface is a thermally stable catalyst with high activity for CO oxidation at 150°C.

Previous reports, both experimental and theoretical ones, involve single metal atoms dispersed on metal, metal oxides and especially two-dimensional (2D) monolayer substrates. These SACs have attracted significant attention due to the large surface area and exceptional properties in catalysis, energy storage and nanoelectronics. Recently, 2D materials (graphene, borophene, hexagonal boron nitride (h-BN), graphitic carbon-nitride, transition metal dichalcogenides (TMDs, e.g. MX_2, M = Mo, W; X = S, Se, Te), black phosphorus (BP), phosphorene, silicene, germanane, etc.) have aroused singnificant interest [38–41]. For example, various 2D materials, such as graphene [42,43], graphyne [44,45], single layer hexagonal BN [46–48], germanane [49–51], phosphorene [52,53], MoS_2 [54,55], WSe_2 [56,57], and other TMD_S [57,58], have been examined as promising substrates for anchoring metal atoms, which could inhibit the isolated metal atoms from agglomeration and provide a specific surface area for adhesive metal atoms as the active site [59].

Among the 2D materials, a new entry of layered early transition metal carbides, nitrides and carbonitrides materials, coined as MXene, has been successfully synthesized by the careful chemical impression of the precursor MAX phases [19,60,61]. The general formula of MAX phase is $M_{n+1}AX_n$, where M represents the early d-block transition metal atom (Sc, Ti, V, Cr; Zr, Nb, Mo; Hf, Ta, W, and so on), A represents the main group's sp-block element (Al, Si, Ge, etc.), and X represents C (carbon) and/or N (nitrogen). By removing the A element, robust layered materials can be made with a general formula of $M_{n+1}X_nT_x$, where T is the surface termination (OH, O, F, S, etc.). In 2011, the first MXene (Ti_3C_2) was synthesized by immersing Ti_3AlC_2 powders in 50% hydrofluoric acid (HF) solution at room temperature [61]. The naked surfaces of MXene materials are chemically active and are often terminated with surface groups such as O, F, and OH groups. The O and OH-terminated MXenes are stable at high temperature, so the OH groups can easily be changed into O terminations and as a result MXenes could be easily prepared experimentally [62–65]. MXenes have been found to have enormous applications within energy storage devices, catalysis, thermoelectric insulators, topological insulators [66,67]. Of particular interest is the finding that MXenes are promising materials for SAC substrate [68–74], especially because they are a type of stable, low-cost materials and can be easily prepared experimentally [75–77].

Inspired by the above studies, we performed quantum chemical calculations using periodic density functional theory (DFT) to investigate the geometries, stability and catalytic behavior of a single cobalt (Co) atom supported on a distinctive MXene (Mo_2CS_2) monolayer. Here the selection of cobalt is based on the abundance, cost and stability of the Co-based catalysts that often feature unpaired electrons at the active center, especially in view of the performance of group-9 metal (Rh and Ir) based catalysts for CO oxidation. Firstly, we investigated the adsorption of O_2, CO and co-adsorption of CO/O_2 on Co_1/Mo_2CS_2. Secondly, three well-known mechanisms, i.e., Eley-Rideal (ER), Langmuir-Hinshelwood (LH) and Termolecular Eley-Rideal (TER) mechanisms, for CO oxidation on Co_1/Mo_2CS_2 were explored systematically. Electronic structure analyses were carried out to determine the activation and reaction mechanism of O_2 and co-adsorbed CO molecule.

THEORETICAL METHODS

The theoretical studies were performed at the level of DFT with the Kohn-Sham spin-polarization formalism. The geometry optimization and energy calculations were carried out by using the Vienna *Ab-initio* Simulation Package (VASP version 5.2) [78,79]. The projector augmented wave (PAW) [80–82] pseudopotentials were used to describe the interaction between core and valence electrons, together with plane wave basis functions with the energy cut-off of 400 eV. The generalized gradient approximation (GGA) with the Perdew-Burke-Ernzerhof (PBE) exchange-correlation functional was employed in these calculations [83,84]. The valence electrons are defined by $4d^45s^2$ for Mo, $3d^74s^2$ for Co, $3s^23p^4$ for S, $2s^22p^4$ for O, and $2s^22p^2$ for C. A cubic supercell of MXene (Mo_2CS_2) was used to build the surface slab. The Mo_2CS_2 monolayer was firstly constructed with a periodic supercell containing 3×3 and 4×4 primitive cell (with 16 C atoms, 32 S atom and 32 Mo atoms). It turned out that both the (3×3) and (4×4) supercells gave almost the same values (Table S1). A vacuum space of 20 Å was used to avoid the interlayer interactions between the substrate and its images. The fully optimized structure of Mo_2CS_2 with fully relaxed positions of atoms is shown in Fig. S1.

For the surface Brillouin zone (BZ) sampling, we used a Monkhorst-Pack (1×1×1) Γ-centered *k*-points grid. The electron density for the ground state was considered to be converged when reaching a total energy threshold of 10^{-5} eV, and all the ions were allowed to relax until the maximum force was less than 0.02 eV Å^{-1}. Atomic charges were computed using Bader's quantum theory of atom-in-molecule (QTAIM) formalism [85,86].

Following the convention of thermodynamics, the binding energy of Co atom on the MXene is defined as

$$E_b[\mathrm{Co}] = E_{tot}[\mathrm{Co_1/MXene}] - E[\mathrm{MXene}] - E[\mathrm{Co}]. \quad (1)$$

The adsorption energy (E_{ads}) of an adsorbate (X) was calculated from the equation:

$$E_{ads} = E_{tot}[\mathrm{X\ldots Co_1/MXene}] - E[\mathrm{Co_1/MXene}] - E(\mathrm{X}), \quad (2)$$

where E_{tot}[X…Co$_1$/MXene], E[Co$_1$/MXene], and E(X) represent the total energy of the X…Co$_1$/MXene adsorption system, Co$_1$/MXene, and free adsorbate, respectively. Moreover, the co-adsorption energies of CO and O_2 were calculated from the equation:

$$\Delta E_{coads} = E_{tot} - E[\mathrm{MXene}] - E[\mathrm{CO}] - E[\mathrm{O_2}]. \quad (3)$$

In order to determine the reaction pathway and energy barriers, the climbing image nudged elastic band (CI-NEB) [87,88] and dimer method [89,90] were applied. All the transition state (TS) geometries were confirmed by having one imaginary vibrational frequency. The energy barrier (E_a) was calculated as $E_a = E_{TS} - E_{IS}$ and the reaction energy was calculated from $\Delta E = E_{FS} - E_{IS}$, where the E_{TS}, E_{IS}, and E_{FS} are the energy of the TS, initial state and final state, respectively. All the other settings used are the default values of the program. By the thermodynamics definition, the positive and negative values represent endothermic and exothermic reactions, respectively.

RESULTS AND DISCUSSION

Geometry and electronic structure of Co_1/Mo_2CS_2 monolayer

In this work, the sulfur-functionalized molybdenum-carbide (Mo_2CS_2) was selected as a support, with Co atom binding on the surface of Mo_2CS_2 to form the SAC of Co_1/Mo_2CS_2. The fully optimized structure of the MXene is presented in Fig. S1 and the local coordination is shown in Scheme 1. There are various binding sites on the surface of Mo_2CS_2 monolayer, such as a top site on the top of sulphur atoms (Site I), a hollow site formed by three neighboring sulphur (S) atoms with a top layer Mo atom (Site II), and a bottom layer of Mo atom (Site III). We optimized the geometries of Co atom binding at the three surface sites and found that the Co single atom prefered to locate at the most stable site on the top of the Mo atom (Site II), consistent with previous studies [72–76].

The optimized geometry of Co_1/Mo_2CS_2 is shown in Fig. 1a. It is found that the Co atom preferred to stay at the energetically most stable site, located above the Mo atoms (Site I) with the binding energy of −3.46 eV, which is around one third of the Co atom's binding energy to phosphotungstic acid (PTA) support [91]. The Co atom is bonded with the three neighboring S atoms, all having equal Co–S bond distance of 2.08 Å. Noticeably, there is significant electron transfer from Co atom to the MXene monolayer, which plays an important role in the strong stabilization of Co single atom on the MXene surface *via* ionic and covalent metal-support interaction (CMSI) [92]. The Bader charge analysis indicates +0.55|*e*| charge on the Co atom and −0.90|*e*| on each neighboring S atom, indicating that the Co atom lies in +II oxidation state when compared with the Bader charge of Co atom in

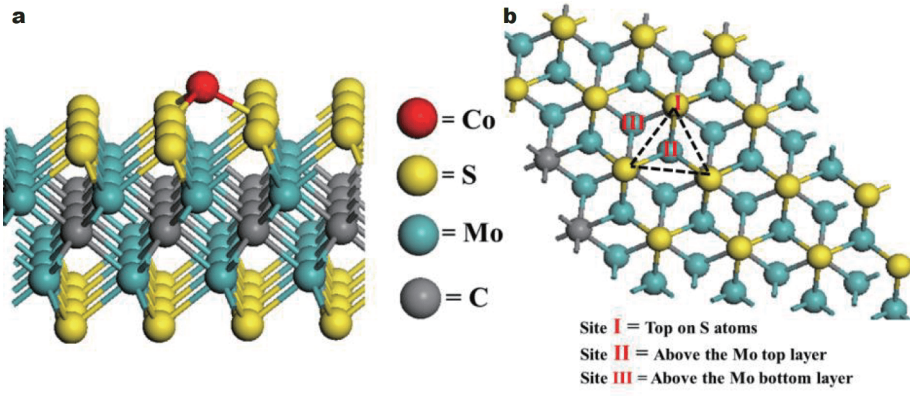

Scheme 1 The local structure of Co_1/Mo_2CS_2 catalyst. (a) Side view of the Co_1 atom binding to the Mo_2CS_2 surface; (b) the possible binding sites (Site I is on top of the S atoms, Sites II and III are above the Mo atoms on the top and bottom layers, respectively).

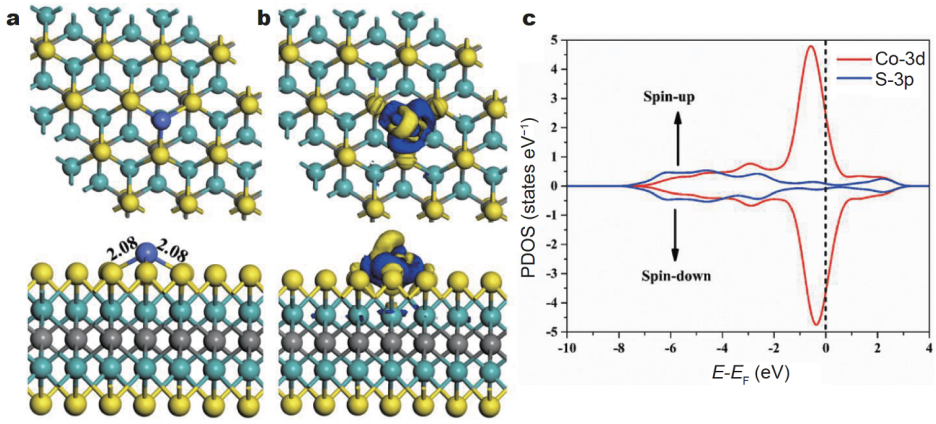

Figure 1 (a) Top and side views of the optimized geometry of Co_1/Mo_2CS_2; (b) PEDD, blue (yellow) isosurface indicates accumulation (depletion) regions. The contour isovalue of the PEDD is ±0.05 a.u. (c) The PDOS projected on Co 3d (red) and S-3p (blue) states. The Fermi level is set to zero.

CoS. The results indicate that electron density transfers from Co atom to the neighboring S atoms, consequently forming partly ionic bonds between the Co–S in Co_1/Mo_2CS_2 monolayer. In addition, the presence of positive charge on Co atom facilitates long-range physisorption of gases (CO, O_2) through charge-induced diploe interaction, and hence the short-range chemisorption through charge-charge ionic interaction due to electron transfer from Co_1/Mo_2CS_2 monolayer to O_2, which results in more effective CO catalytic oxidation. The calculated partial electron density differences (PEDD) of Co_1/Mo_2CS_2 are shown in Fig. 1b, which exhibit significant electron depletion and electron accumulation region between Co and its neighboring S atoms. It is clear that there is a loss of electron density above the embedded Co atom, consistent with the electron density flowing from Co atom towards the nearest S atoms. The PEDD results are also in good agreement with the Bader charge analysis. Besides, strong interactions between the Co atom and its neighboring S atoms are also verified by the partial density of states (PDOS) calculated for Co_1/Mo_2CS_2, as shown in Fig. 1c. It is found that the Co atom shows main peak near the Fermi level (E_F) with limited spin polarization. The strong covalent interactions between the Co and S atoms can be confirmed by the overlapping peaks, where the 3d-orbital of Co merges with the 3p-orbital of S atom, indicating higher reactivity of Co_1/Mo_2CS_2 monolayer. However, presence of Co 3d orbital charcaters near the Fermi level shows high reactivity and may play a role in activating the adsorbates during the catalytic reaction. The ferromagnetic and anti-ferromagnetic coupling of the unpaired electrons on Co and Mo shows little energy difference (~0.03 eV).

As has been shown before, single metal atoms might migrate from one site to another during reaction [93–95]. While Co has a binding energy of 3.46 eV on the catalyst surface, the Co_1/Mo_2CS_2 SAC is only meta-stable, with a formation energy ~2 eV when reference to the cohesive energy of Co atoms in the hexagonal close packed (HCP) bulk cobalt metal and Mo_2CS_2, as is often the case for various SACs. To reveal the intrinsic stability of the embedded single Co atom, we also calculated the migration barrier of the Co atom on the Mo_2CS_2 (MXene) monolayer from the most preferable site to its neighboring site. The migration barrier was determined as the energy difference between the metastable structure and the most preferable stable site. The migration energy profile is displayed in Fig. S2. One can see that this single-atom migration process is not only endothermic by 0.46 eV, but also having an energy barrier as high as 1.21 eV, which makes the migration of Co atom on the MXene surface rather difficult at room temperature or below. The moderately high migration barrier indicates the relative immobility of the embedded Co atom on the Mo_2CS_2 surface, especially at low temperature. Therefore, we conclude that single Co atom embedded on Mo_2CS_2 surface tends to be stable at ambient temperature and Co clustering is neither thermodynamically nor kinetically favored under such circumstances.

Adsorption of reaction species (CO, O_2) on Co_1/Mo_2CS_2 monolayer

In order to explore the mechanism of CO oxidation on the SAC, the adsorption and co-adsorption properties of the reactant species (CO and O_2) were investigated. The most stable adsorption configuration of CO on Co_1/Mo_2CS_2 is shown in Fig. 2a, where CO is strongly bonded

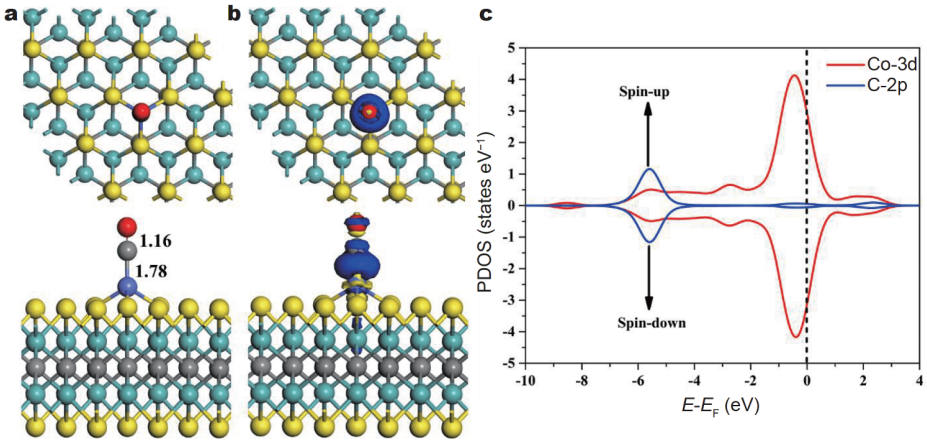

Figure 2 (a) Top and side views of the optimized geometry of CO adsorbed on Co_1/Mo_2CS_2 monolayer. (b) PEDD, blue (yellow) isosurface indicates accumulation (depletion) regions. The contour value of the PEDD is ±0.05 a.u. (c) The PDOS projected on Co 3d (red) and C 2p (blue) states. The Fermi level is set to zero.

to Co dopant with the end-on configuration. The calculated adsorption energy of CO is −1.85 eV, which is 0.45 eV stronger than that of O_2 adsorption, suggesting favorable adsorption of CO than that of O_2. The calculated bond length of Co–C is 1.78 Å, while a slight elongation of C–O bond length from 1.13 (free CO) to 1.16 Å reveals reasonable activation of C–O bond. In addition, strong adsorption between the Co and CO molecule occurs *via* the donation and back-donation bonding model of Dewar-Chatt-Duncanson (DCD) [96,97]. On the one hand, the lone pair of CO donates to the vacant 3d/4s orbitals of Co atom, and on the other hand the occupied Co 3d orbital interacts with the $2\pi^*$ orbital of the CO molecule, initiating a reverse charge transfer from the Co center to the CO molecule. The Bader charge analysis reveals a significant charge redistribution, with −0.24|*e*| on the CO molecule and +0.60|*e*| on the Co atom, which indicates the charge transfer from Co_1/Mo_2CS_2 to the CO molecule. The charge density transfer occurs from Co 3d orbital to $2\pi^*$ antibonding orbital of CO molecule, which causes elongation of C–O bond length (from 1.13 to 1.16 Å). This result is also confirmed by the PEDD displayed in Fig. 2b. The adsorption of CO onto Co_1/Mo_2CS_2 is primarily attributed to the 5σ electrons donated to the Co 3d orbital and back-donation of the filled Co 3d electrons to the antibonding $2\pi^*$ orbital of CO. In order to understand the electron density, and transfer between the Co_1/Mo_2CS_2 and CO molecule, PDOS analysis was projected between the Co 3d and CO 2p orbitals. As shown in Fig. 2c, it is clear that the interaction between the Co atom and CO molecule is mainly due to the strong overlap of the Co 3d orbital with the $2\pi^*$ orbital of CO. Upon CO adsorption, CO-$2\pi^*$ orbitals are also partially occupied because some electrons transfer from Co to CO-$2\pi^*$. The charge transfers and the strong hybridization of the Co atom and CO molecule lead to the elongation of the C–O bond.

Fig. 3a illustrates the most stable adsorption configuration of O_2 on Co_1/Mo_2CS_2 monolayer with the corresponding adsorption energy of −1.40 eV (exothermic). Compared with the adsorption of CO, the O_2 adsorption alone is weaker by 0.45 eV, suggesting the preferential adsorption of CO than that of O_2. The bond distances of Co–O1 and Co–O2 are 1.79 and 1.92 Å, respectively, and the bond distance of O–O is slightly elongated from 1.23 (free O_2) to 1.36 Å (superoxide). The Bader charge analysis indicates that 0.79|*e*| charge is transferred from Co_1/Mo_2CS_2 to O_2 molecule. Therefore, the electron density transfer occurs from Co 3d orbital to antibonding $2\pi^*$ orbital of O_2, which demonstrates the significant elongation of O–O bond and the activation of O_2 into a superoxide (O_2^-) ligand. Hence, Co_1/Mo_2CS_2 acts as the electron donor, while O_2 molecule acts as the electron acceptor. To further confirm such electron transfer behavior, we also considered the PEDD plots of the O_2 adsorption over Co_1/Mo_2CS_2, as shown in Fig. 3b. The electron density accumulation regions are rendered in blue color, covering the Co and O_2 atoms, clearly showing the electron transfer from Co_1/Mo_2CS_2 to O_2. Fig. 3c displays the PDOS for the 3d orbital of Co atom and the 2p orbital of adsorbed O_2 atoms. The strong hybridization between these two kinds of orbitals can be clearly seen from the PDOS, which exhibit substantial weakening of the O–O bond, facilitating CO oxidation through O_2

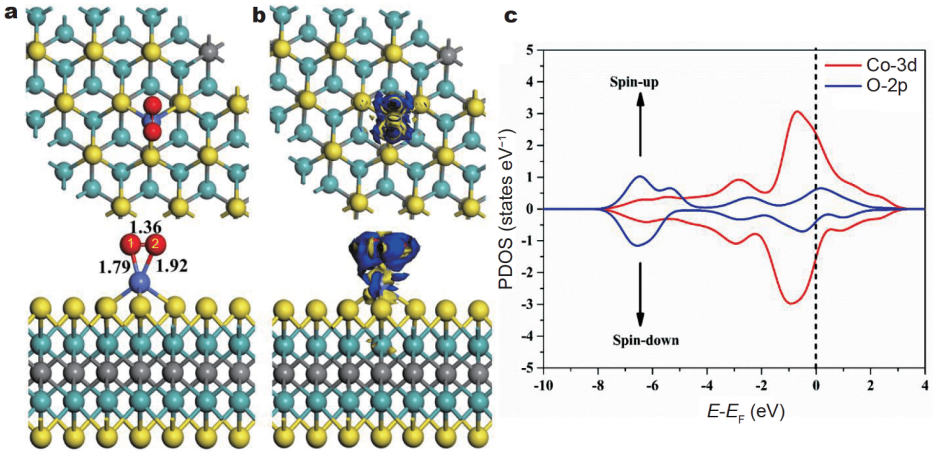

Figure 3 (a) Top and side views of the optimized geometry of O_2 adsorbed on Co_1/MXene monolayer *via* a side-on configuration. (b) PEDD, blue (yellow) isosurface indicates accumulation (depletion) region. The contour value of the PEDD is ±0.05 a.u. (c) The PDOS projected on Co 3d (red) and O 2p (magenta) states. The Fermi level is set to zero.

molecule activation.

From the above discussion, one can see that for individual adsorption configuration of the gas molecules (CO and O_2) on Co_1/Mo_2CS_2, the CO adsorption configuration on Co_1/Mo_2CS_2 is stronger and preferable as compared with that of O_2. Moreover, when a CO molecule is pre-adsorbed on Co_1/Mo_2CS_2, the co-adsorption of the second CO or O_2 molecules on the active site will have a significant effect on the consequent reaction path. Fig. 4 illustrates the most stable co-adsorption configuration of two CO molecules and CO+O_2 molecules on Co_1/Mo_2CS_2, where the oxygen atom of O_2 adsorbs with end-on configuration over Co_1/Mo_2CS_2. The co-adsorption binding energies of two CO molecules and CO+O_2 molecules on Co_1/MXene are −2.83 and −2.09 eV, respectively. Higher co-adsorption energies of two CO molecules and CO+O_2 molecules than the isolated CO (−1.85 eV) and O_2 (−1.40 eV) adsorption suggest that the co-adsorption is more feasible. Besides, with respect to binding energies, the co-adsorption of two CO molecules is preferable than that of CO+O_2 molecules on Co_1/Mo_2CS_2. The respective electron density differences of CO+O_2 molecules and two CO molecules on Co_1/Mo_2CS_2 are shown in Fig. 4b, d. It shows significant charge accumulation and depletion regions between Co atom and adsorbed CO+O_2 molecules or the two CO molecules. According to the computational results, the co-adsorbed configuration *via* the C atom of CO over the Co_1/MXene is the most energetically favorable configuration, as shown in Fig. 4c.

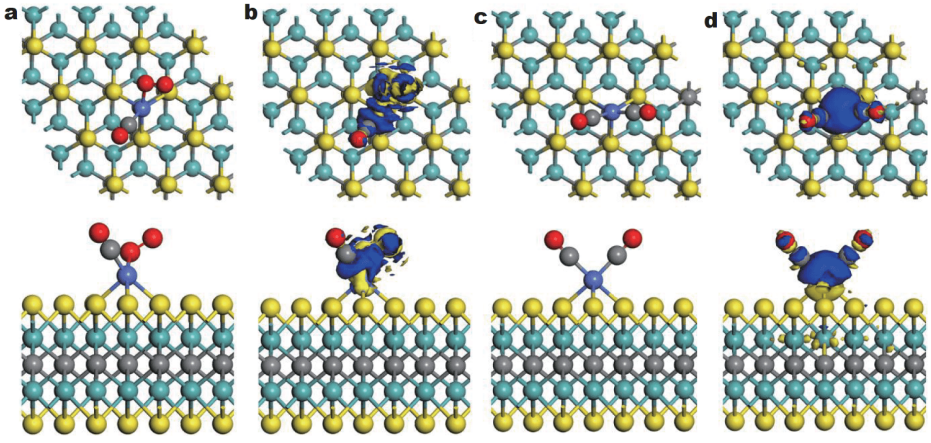

Figure 4 (a) Top and side views of the optimized geometry of co-adsorption of CO+O_2; (c) two CO molecules co-adsorbed on Co_1/Mo_2CS_2 monolayer; (b, d) PEDD, blue (yellow) isosurface indicates accumulation (depletion) region; (c) the contour value of the PEDD is ±0.05 a.u.

CO oxidation catalyzed $Co_1/MXene$ monolayer

In general, CO oxidation reaction could take place *via* two well-known traditional mechanisms, namely the ER and the LH mechanism. The ER mechanism proceeds with a gas phase CO molecule, which interacts with the pre-adsorbed and activated O_2 to form CO_2. In LH mechanism, the reaction starts with the co-adsorption of CO and O_2 molecules on the Co_1/Mo_2CS_2 site leading to the formation and dissociation of peroxide-like (OCOO) IM, which finally decomposes to CO_2. Subsequently, the adsorption energy of CO (−1.85 eV) is slightly higher than that of O_2 (−1.40 eV) over Co_1/Mo_2CS_2, and the co-adsorption energy of O_2 and CO molecules (−2.09 eV) is higher than the isolated O_2 and CO adsorption, as mentioned earlier. Thus, both ER and LH mechanisms for the CO oxidation reaction on Co_1/Mo_2CS_2 are possible.

Recently, Mao *et al.* [98] presented a mechanism for CO oxidation, namely TER mechanism. In TER mechanism, the reaction starts with a free O_2 molecule activated by two CO molecules co-adsorbed on the Co_1/Mo_2CS_2, forming an OCO-Co-OCO IM which dissociates to two CO_2 molecules. The co-adsorption energy of two CO molecules (−2.83 eV) is markedly higher than that of the co-adsorption energy of CO and O_2 molecules (−2.09 eV) over the Co_1/Mo_2CS_2, suggesting that TER mechanism is dominant for CO oxidation over the Co_1/Mo_2CS_2 monolayer.

LH mechanism

Fig. 5 depicts the optimized structure of the corresponding stationary points as well as the potential energy profile for CO oxidation through the LH mechanism. We chose the most stable CO and O_2 co-adsorption configuration as initial structure (IS1), where both CO and O_2 are highly activated over Co_1/Mo_2CS_2. The co-adsorption energy of CO and O_2 is −2.09 eV, which is higher than those of the isolated CO (−1.85 eV) and O_2 (−1.40 eV) adsorption, indicating the more feasible co-adsorption of CO and O_2 over Co_1/Mo_2CS_2. In the catalytic reaction, after the co-adsorption of CO and O_2 over Co_1/Mo_2CS_2, one of the O atom of O_2 starts interacting with the C atom of CO to form a peroxide-like (OOCO) intermediate (IM1) through the transition state (TS1), with significant elongation of O–O bond length from 1.29 to 1.52 Å (peroxide) and the formation of new C–O bond (1.35 Å) between the CO and O_2. The calculated activation energy barrier from IS1 to IM1 is 0.78 eV, with one imaginary frequency of 449i cm^{-1}, and this is the rate-limiting step of the LH mechanism. Notably, when the IM1 is formed, the catalytic dissociation process is easy to occur. Subsequently, cleavage of O–O bond in the peroxide-like (OOCO) IM yields CO_2 molecule and retains the adsorbed oxygen (O_a) atom through a TS2 state, which has an activation energy barrier of only 0.17 eV and exothermic reaction energy of −2.15 eV. TS2 has been confirmed by one imaginary frequency of 200i cm^{-1}, which is associated with the formation of C–O bond and dissociation of O–O bond. Likewise, because of relatively weak adsorption and large distance from the O-Co_1/Mo_2CS_2, the formed CO_2 molecule will be spontaneously desorbed at room temperature.

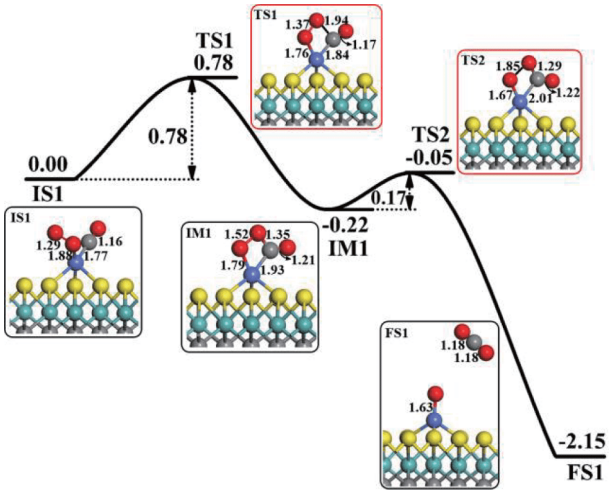

Figure 5 Schematic energy profile and optimized structure of the corresponding stationary points for CO oxidation catalyzed by Co_1/Mo_2CS_2 *via* LH mechanism. Hereafter, the TSs are marked with red lines. All energies are given in eV, and bond lengths are specified in Å.

ER mechanisms

The optimized geometries concerning the ER mechanism, including the IS, TS, FS and the reaction energy profile are presented in Fig. 6. The physisorbed CO above the pre-adsorbed O_2 over Co_1/Mo_2CS_2 is selected as an initial structure (IS2), in which the bond distance between the C atom and one O atom of O_2 is 3.19 Å. In the catalytic reaction, the C atom of CO interacts with one of the O atoms of the pre-adsorbed O_2 molecule, resulting in the breaking of the Co–O bond and the formation of CO_2 molecule (FS1) through the transition state (TS3). Here TS3 has an activation energy barrier of 0.88 eV with one imaginary frequency of 662i cm^{-1}, which is associated with the formation of C–O bond and the dissociation of O–O bond.

During the second ER step, the second CO molecule approaches to the surface and interacts with the adsorbed O_a atom from the first step. The reaction energy profile

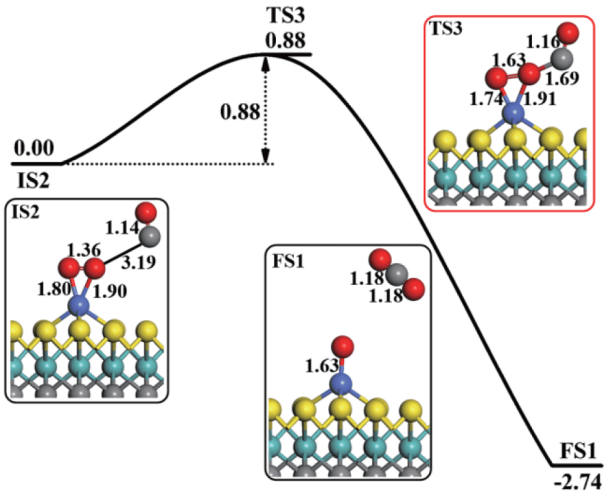

Figure 6 Schematic energy profile and optimized structure of the corresponding stationary points for CO oxidation catalyzed by Co_1/Mo_2CS_2 *via* ER mechanism. Hereafter, the TS is marked with red lines. All energies are given in eV, and bond lengths are specified in Å.

and structures of the second ER path are shown in Fig. 7. The CO molecule physisorbed on parallel configuration over O_a atom pre-adsorbed on Co_1/Mo_2CS_2 is selected as an initial structure (IS3), in which the bond distance between the C atom and one O_a is 3.64 Å. The CO molecule reacts with the remaining O_a atom over Co_1/Mo_2CS_2 to produce the second CO_2 molecule (FS2) through TS4 (imaginary frequency 283i cm^{-1}) and the catalyst is recovered in the catalytic cycle. The calculated reaction energy barrier and exothermic reaction energies are 0.17 and −2.47 eV, respectively.

TER mechanism

As mentioned above, termolecular TER mechanism is a novel mechanism for CO oxidation as is found on the single Pd and Au atoms anchored on an h-BN sheet [98,99]. The potential energy profile and the optimized structure of the IS, IM, TSs and FS are presented in Fig. 8. Remarkably, the co-adsorption of two CO molecules over Co_1/Mo_2CS_2 is stronger than the isolated CO and O_2 molecules, which is selected as an initial structure (IS4). In IS4, a physisorbed O_2 molecule drifts above the chemically co-adsorbed two CO molecules on the Co atom, in which the distance between the C···O (physisorbed O_2 and chemically co-adsorbed CO molecules) is 4.08 and 3.91 Å, respectively. In the catalytic reaction, the physisorbed O_2 molecule is activated when approaching the two co-adsorbed CO molecules and leads to the formation of the OCO-Co-OCO intermediate (IM2), which has a pentagonal ring configuration through the transition state (TS5, imaginary frequency 965i cm^{-1}). The corresponding energy barrier (TS5) of the reaction step is calculated to be 0.53 eV and the reaction is exothermic by −0.38 eV. In this process, the distance between two newly formed C–O bonds, between the C and physisorbed O_2 molecule, gradually decreases and the O–O bond is elongated from 1.23 to 1.47 Å (peroxide). Successively, with the cleavage of O–O bond, the OCO-Co-OCO IM dissociates into two CO_2 molecules *via* transition state

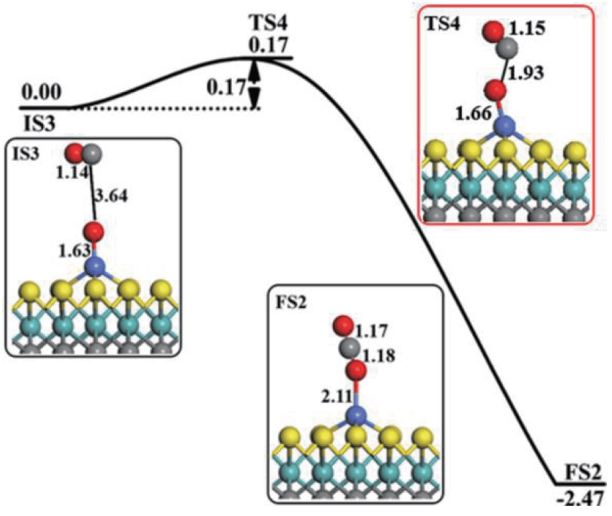

Figure 7 Schematic energy profile and optimized structure of the corresponding stationary points for CO oxidation catalyzed by Co_1/Mo_2CS_2 *via* the second ER step mechanism. Hereafter, the TS is marked with red lines. All energies are given in eV, and bond lengths are specified in Å.

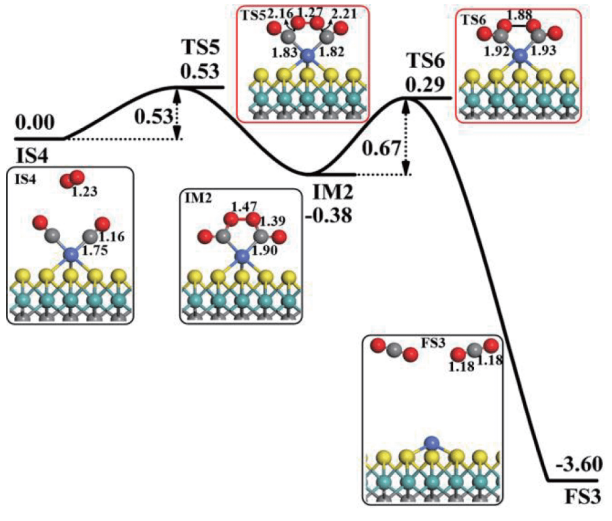

Figure 8 Schematic energy profile and optimized structure of the corresponding stationary points for CO oxidation catalyzed by Co_1/Mo_2CS_2 *via* TER mechanism. Hereafter, the TSs are marked with red lines. All energies are given in eV, and bond lengths are specified in Å.

TS6 (imaginary frequency 238i cm^{-1}), which has an activation energy barrier of 0.67 eV and the exothermic reaction energy of −3.60 eV. This step is the rate-limiting step of the TER reaction mechanism.

Furthermore, the calculated adsorption energy of the formed CO_2 molecules is −0.17 eV, signifying that the newly formed CO_2 molecules can be easily released into the air at low temperature and the Co_1/Mo_2CS_2 monolayer system is restored and ready for a new cycle of CO oxidation. So the key point is the comparison of co-adsorption energies between two CO (−2.83 eV) molecules with CO+O_2 (−2.09 eV) molecules and the isolated CO (−1.85 eV) and O_2 (−1.40 eV), which suggests that the TER mechanism is more feasible over Co_1/Mo_2CS_2 catalyst.

For the TER mechanism, the reaction energy barrier (0.67 eV) of the rate-limiting step is found to be relatively lower than that of the common LH and ER mechanism. The electronic structure study was carried out to further elucidate the origin of the TER mechanism of CO oxidation over Co_1/Mo_2CS_2. Fig. 9a–c illustrate the electronic configuration analysis of the PDOS of the initial state (IS4), IM2 and transition state (TS5) of TER mechanism. In Fig. 9c, the antibonding $2\pi^*$ orbital of O_2 is partially filled, which activates the O_2 molecule and weakens the O–O bond. Additionally, as a comparison with the initial structure (IS4), the 2p orbital of O_2 in TS5 overlaps with the 2p orbital of C atom, which validates the circumstance that the O_2 molecule can be activated by the co-adsorbed CO molecules. To gain more insights about the activation of O_2 molecule by the co-adsorbed CO molecule, frontier molecular orbital analysis is performed, as shown in Fig. 9d. It is clear that the lowest occupied molecular orbitals (LUMO) of the physisorbed O_2 molecule match with the highest occupied molecular orbital (HOMO) of the chemically adsorbed two CO molecules over Co_1/Mo_2CS_2 monolayer, which facilitates electron transfer to the antibonding $2\pi^*$ orbital of O_2 and weakening of the O–O bond.

To summarize, the rate-limiting step for the formation of two CO molecules from the dissociation of OCO-Co-OCO IM has an energy barrier of only 0.67 eV. The small energy barrier and high exothermicity indicate high catalytic activity of the Co_1/Mo_2CS_2 monolayer toward the CO oxidation reaction through the TER reaction mechanism. The positively charged C atoms of the co-adsorbed two CO molecules can help to anchor the negatively charged O_2 molecule. Comparing TER with LH and ER mechanisms, the rate-limiting steps energy barriers are 0.67, 0.78 and 0.88 eV, respectively, suggesting that the TER mechanism would be more favorable than the LH and ER ones for CO oxidation over Co_1/Mo_2CS_2 monolayer.

In addition, the spin magnetic moments can provide useful information for the elementary steps involved in the Co oxidation reaction. From the calculated spin

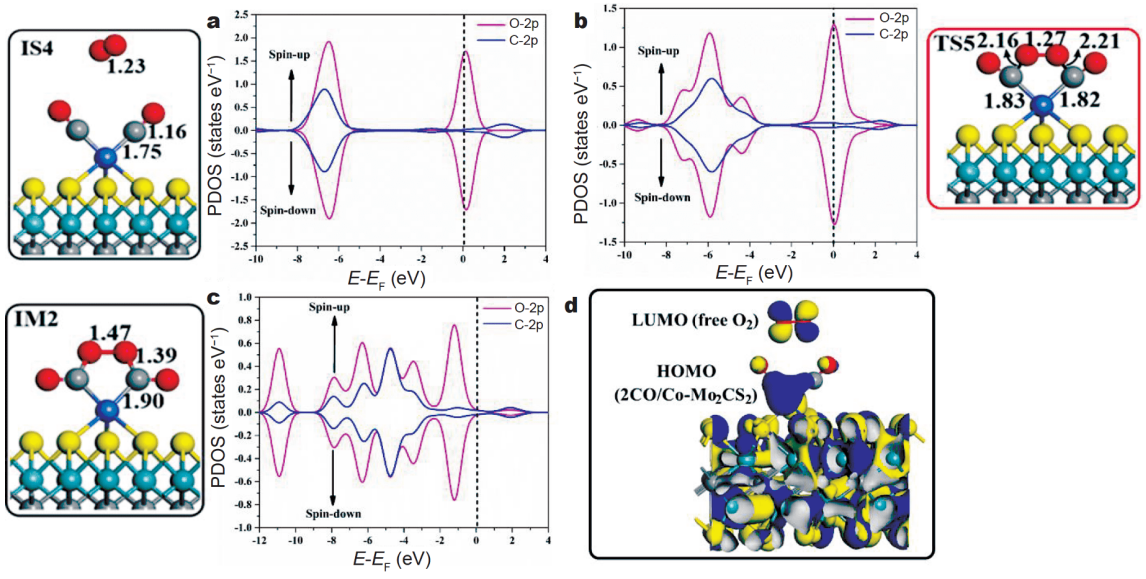

Figure 9 (a–c) The PDOS projected initial state (IS4), transition state (TS5) and IM2 on C 2p (blue) and O 2p (magenta) states. The Fermi level is set to zero. (d) Front view of the HOMOs of two co-adsorbed COs and LUMO of the physisorbed O_2 on Co_1/Mo_2CS_2. The isosurface is set to be 0.01 e $Å^{-3}$.

magnetic moments, the Co_1/Mo_2CS_2 catalyst has the spin magnetic moments of $-0.77\mu_B$ for the systems with three unpaired electrons and $0.31\mu_B$ for one unpaired electron on Co_1 atom (see Fig. S3). The total magnetic moments of both systems are $2.00\mu_B$. The calculated magnetic moment of all the elementary steps involved in the CO oxidation *via* (ER, LH and TER) mechanisms are presented in Table S2, which shows that the magnetic moment changes in all the steps up to the release of CO_2 molecule. We have also calculated the PDOS of all the elementary steps and the results are presented in Figs S4–S7. It can be seen that Co 3d orbital plays an important role in changing the oxidation state and magnetic moment of Co in all the elementary steps near the Fermi level.

CONCLUSIONS

The first-principles DFT calculations using PBE functional has been used to investigate the CO oxidation by O_2 over Co_1/Mo_2CS_2. The results show that isolated single Co atom can strongly anchor to the defective Mo_2CS_2 monolayer, and suggest that Co_1/Mo_2CS_2 possesses robust stability and attractive low-temperature catalytic activity towards the CO oxidation. The adsorption energy and charge transfer of CO and O_2 molecules adsorbed over Co_1/Mo_2CS_2 were calculated and discussed in details. It is found that the CO adsorption is more favorable than O_2 adsorption over Co_1/Mo_2CS_2. The CO oxidation reaction mechanisms were studied over Co_1/Mo_2CS_2 *via* two traditional LH and ER mechanisms and a recently proposed TER mechanism. The rate-limiting step is O_2(ad)+CO(ad)→OOCO(ad) with the activation energy barrier of 0.78 eV for the LH mechanism, O_2(ad)+CO(gas)→CO_2(gas)+O(ad) with the activation energy barrier of 0.88 eV for ER mechanism, and the dissociation of IM OCO-Co-OCO(ad)→$2CO_2$ (gas) with an activation energy barrier of 0.67 eV for TER mechanism. The relatively small activation energy barriers for the LH, ER and TER mechanisms, suggest that all these mechanisms are possible to occur at low temperatures. However, the TER mechanism featuring a fascinating OC(OO)CO IM adsorbed on Co is, to a certain degree, more preferable with the lowest energy barrier when compared with the LH and ER mechanisms. The charge transfers from Co 3d orbitals, with the assistance of 2p orbitals of CO, to antibonding $2\pi^*$ orbital of O_2, lead to the activation of O_2 molecule and weakening of the O–O bond. Our findings suggest that the MXene based Co_1/Mo_2CS_2 catalyst is one of the promising SACs for low-temperature CO oxidation. Inasmuch as the strong Co–S bonding and the facile interchangeable feature of Co(II/III) oxidation states, cobalt-based MXene catalysts might be advantageous for redox reactions. The highly stable MXene materials appear to be ideal substrates for anchoring various single metal atoms due to strong binding with the surface termination (OH, O, F, S, etc.) ligands. These outcomes provide useful intimations for experimentalists to develop non-noble metal SACs for the CO oxidation reaction.

Received 22 June 2020; accepted 6 July 2020; published online 9 September 2020

1 Bunluesin T, Cordatos H, Gorte RJ. Study of CO oxidation kinetics on Rh/ceria. J Catal, 1995, 157: 222–226
2 Gong XQ, Liu ZP, Raval R, *et al.* A systematic study of CO oxidation on metals and metal oxides: Density functional theory calculations. J Am Chem Soc, 2004, 126: 8–9
3 Falsig H, Hvolbæk B, Kristensen I , *et al.* Trends in the catalytic CO oxidation activity of nanoparticles. Angew Chem, 2008, 120: 4913–4917
4 Lim FCH, Zhang J, Jin H, *et al.* A density functional theory study of CO oxidation on Pd-Ni alloy with sandwich structure. Appl Catal A-General, 2013, 451: 79–85
5 Esrafili MD, Saeidi N. Sn-embedded graphene: An active catalyst for CO oxidation to CO_2? Phys E-Low-dimensional Syst NanoStruct, 2015, 74: 382–387
6 Alavi A, Hu P, Deutsch T, *et al.* CO oxidation on Pt(111): An *ab initio* density functional theory study. Phys Rev Lett, 1998, 80: 3650–3653
7 Chen MS, Cai Y, Yan Z, *et al.* Highly active surfaces for CO oxidation on Rh, Pd, and Pt. Surf Sci, 2007, 601: 5326–5331
8 Liu L, Zhou F, Wang L, *et al.* Low-temperature CO oxidation over supported Pt, Pd catalysts: Particular role of FeO_x support for oxygen supply during reactions. J Catal, 2010, 274: 1–10
9 Stuve EM, Madix RJ, Brundle CR. CO oxidation on Pd(100): A study of the coadsorption of oxygen and carbon monoxide. Surf Sci, 1984, 146: 155–178
10 Zhang CJ, Hu P. CO oxidation on Pd(100) and Pd(111): A comparative study of reaction pathways and reactivity at low and medium coverages. J Am Chem Soc, 2001, 123: 1166–1172
11 Molina LM, Hammer B. Active role of oxide support during CO oxidation at Au/MgO. Phys Rev Lett, 2003, 90: 206102
12 Su HY, Yang MM, Bao XH, *et al.* The effect of water on the CO oxidation on Ag(111) and Au(111) surfaces: A first-principle study. J Phys Chem C, 2008, 112: 17303–17310
13 Ghosh TK, Nair NN. Rh_1/γ-Al_2O_3 single-atom catalysis of O_2 activation and CO oxidation: Mechanism, effects of hydration, oxidation state, and cluster size. ChemCatChem, 2013, 5: 1811–1821
14 Zhang LL, Sun MJ, Liu CG. CO oxidation on the phosphotungstic acid supported Rh single-atom catalysts *via* Rh-assisted Mars-van Krevelen mechanism. Mol Catal, 2019, 462: 37–45
15 Gao F, Goodman DW. Model catalysts: Simulating the complexities of heterogeneous catalysts. Annu Rev Phys Chem, 2012, 63: 265–286
16 Liu JC, Wang YG, Li J. Toward rational design of oxide-supported single-atom catalysts: Atomic dispersion of gold on ceria. J Am Chem Soc, 2017, 139: 6190–6199
17 Li J, Li Y, Zhang T. Recent progresses in the research of single-atom catalysts. Sci China Mater, 2020, 63: 889–891

18 Li J, Liu J, Zhang T. Preface to the special issue of the international symposium on single-atom catalysis (ISSAC-2016). Chin J Catal, 2017, 38: 1431
19 Zhang X, Lei J, Wu D, *et al.* A Ti-anchored Ti_2CO_2 monolayer (MXene) as a single-atom catalyst for CO oxidation. J Mater Chem A, 2016, 4: 4871–4876
20 Heiz U, Sanchez A, Abbet S, *et al.* Catalytic oxidation of carbon monoxide on monodispersed platinum clusters: Each atom counts. J Am Chem Soc, 1999, 121: 3214–3217
21 Lin J, Qiao B, Liu J, *et al.* Design of a highly active Ir/Fe(OH)$_x$ catalyst: Versatile application of Pt-group metals for the preferential oxidation of carbon monoxide. Angew Chem, 2012, 124: 2974–2978
22 Lei Y, Mehmood F, Lee S, *et al.* Increased silver activity for direct propylene epoxidation *via* subnanometer size effects. Science, 2010, 328: 224–228
23 Qiao B, Wang A, Yang X, *et al.* Single-atom catalysis of CO oxidation using Pt_1/FeO_x. Nat Chem, 2011, 3: 634–641
24 Yang XF, Wang A, Qiao B, *et al.* Single-atom catalysts: A new frontier in heterogeneous catalysis. Acc Chem Res, 2013, 46: 1740–1748
25 Wang A, Li J, Zhang T. Heterogeneous single-atom catalysis. Nat Rev Chem, 2018, 2: 65–81
26 Liu JC, Tang Y, Wang YG, *et al.* Theoretical understanding of the stability of single-atom catalysts. Natl Sci Rev, 2018, 5: 638–641
27 Li Z, Chen Y, Ji S, *et al.* Iridium single-atom catalyst on nitrogen-doped carbon for formic acid oxidation synthesized using a general host-guest strategy. Nat Chem, 2020, 12: 764–772
28 Zhao S, Chen F, Duan S, *et al.* Remarkable active-site dependent H_2O promoting effect in CO oxidation. Nat Commun, 2019, 10: 3824
29 He Y, Liu JC, Luo L, *et al.* Size-dependent dynamic structures of supported gold nanoparticles in CO oxidation reaction condition. Proc Natl Acad Sci USA, 2018, 115: 7700–7705
30 Liang J, Lin J, Liu J, *et al.* Dual metal active sites in an Ir_1/FeO_x single-atom catalyst: A redox mechanism for the water-gas shift reaction. Angew Chem Int Ed, 2020, 59: 12868–12875
31 Wang L, Huang L, Liang F, *et al.* Preparation, characterization and catalytic performance of single-atom catalysts. Chin J Catal, 2017, 38: 1528–1539
32 Chen Y, Ji S, Chen C, *et al.* Single-atom catalysts: Synthetic strategies and electrochemical applications. Joule, 2018, 2: 1242–1264
33 Sun S, Zhang G, Gauquelin N, *et al.* Single-atom catalysis using Pt/graphene achieved through atomic layer deposition. Sci Rep, 2013, 3: 1775
34 Yan H, Cheng H, Yi H, *et al.* Single-atom Pd_1/graphene catalyst achieved by atomic layer deposition: Remarkable performance in selective hydrogenation of 1,3-butadiene. J Am Chem Soc, 2015, 137: 10484–10487
35 Thang HV, Pacchioni G, DeRita L, *et al.* Nature of stable single atom Pt catalysts dispersed on anatase TiO_2. J Catal, 2018, 367: 104–114
36 Li X, Bi W, Zhang L, *et al.* Single-atom Pt as co-catalyst for enhanced photocatalytic H_2 evolution. Adv Mater, 2016, 28: 2427–2431
37 Nie L, Mei D, Xiong H, *et al.* Activation of surface lattice oxygen in single-atom Pt/CeO_2 for low-temperature CO oxidation. Science, 2017, 358: 1419–1423
38 Deng D, Novoselov KS, Fu Q, *et al.* Catalysis with two-dimensional materials and their heterostructures. Nat Nanotech, 2016, 11: 218–230
39 Chia X, Pumera M. Characteristics and performance of two-dimensional materials for electrocatalysis. Nat Catal, 2018, 1: 909–921
40 Anasori B, Lukatskaya MR, Gogotsi Y. 2D metal carbides and nitrides (MXenes) for energy storage. Nat Rev Mater, 2017, 2: 16098
41 Li WL, Chen X, Jian T, *et al.* From planar boron clusters to borophenes and metalloborophenes. Nat Rev Chem, 2017, 1: 71
42 Zhang XL, Yamada H, Saito T, *et al.* Development of hydrogen-selective triphenylmethoxysilane-derived silica membranes with tailored pore size by chemical vapor deposition. J Membrane Sci, 2016, 499: 28–35
43 Wang M, Wang Z. Single Ni atom incorporated with pyridinic nitrogen graphene as an efficient catalyst for CO oxidation: First-principles investigation. RSC Adv, 2017, 7: 48819–48824
44 Wu P, Du P, Zhang H, *et al.* Graphyne-supported single Fe atom catalysts for CO oxidation. Phys Chem Chem Phys, 2015, 17: 1441–1449
45 Lin ZZ. Graphdiyne-supported single-atom Sc and Ti catalysts for high-efficient CO oxidation. Carbon, 2016, 108: 343–350
46 Yin CG, Ma Y, Liu ZJ, *et al.* Multifunctional boron nitride nanosheet/polymer composite nanofiber membranes. Polymer, 2019, 162: 100–107
47 Zeng H, Zhi C, Zhang Z, *et al.* "White graphenes": Boron nitride nanoribbons *via* boron nitride nanotube unwrapping. Nano Lett, 2010, 10: 5049–5055
48 Li M, Li Y, Zhou Z, *et al.* Metal-decorated defective BN nanosheets as hydrogen storage materials. Front Phys, 2011, 6: 224–230
49 Liu G, Lei XL, Wu MS, *et al.* Comparison of the stability of free-standing silicene and hydrogenated silicene in oxygen: A first principles investigation. J Phys-Condens Matter, 2014, 26: 355007
50 Bianco E, Butler S, Jiang S, *et al.* Stability and exfoliation of germanane: A germanium graphane analogue. ACS Nano, 2013, 7: 4414–4421
51 Dávila ME, Xian L, Cahangirov S, *et al.* Germanene: A novel two-dimensional germanium allotrope akin to graphene and silicene. New J Phys, 2014, 16: 095002
52 Lin JH, Zhang H, Cheng XL. First-principle study on the optical response of phosphorene. Front Phys, 2015, 10: 1–9
53 Zhu Z, Chen C, Liu J, *et al.* The electronic and optical properties of Au doped single-layer phosphorene. Russ J Phys Chem, 2018, 92: 132–139
54 Mao J, Wang Y, Zheng Z, *et al.* The rise of two-dimensional MoS_2 for catalysis. Front Phys, 2018, 13: 138118
55 Lukowski MA, Daniel AS, Meng F, *et al.* Enhanced hydrogen evolution catalysis from chemically exfoliated metallic MoS_2 nanosheets. J Am Chem Soc, 2013, 135: 10274–10277
56 Wang T, Andrews K, Bowman A, *et al.* High-performance WSe_2 phototransistors with 2D/2D Ohmic contacts. Nano Lett, 2018, 18: 2766–2771
57 Allain A, Kis A. Electron and hole mobilities in single-layer WSe_2. ACS Nano, 2014, 8: 7180–7185
58 Huang X, Zhang H. Molecular crystals on two-dimensional van der Waals substrates. Sci China Mater, 2015, 58: 5–8
59 Ahmed S, Yi J. Two-dimensional transition metal dichalcogenides and their charge carrier mobilities in field-effect transistors. Nano-Micro Lett, 2017, 9: 50
60 Naguib M, Come J, Dyatkin B, *et al.* MXene: A promising transition metal carbide anode for lithium-ion batteries. Electrochem

Commun, 2012, 16: 61–64
61 Naguib M, Kurtoglu M, Presser V, *et al.* Two-dimensional nanocrystals produced by exfoliation of Ti_3AlC_2. Adv Mater, 2011, 23: 4248–4253
62 Naguib M, Mochalin VN, Barsoum MW, *et al.* 25th anniversary article: MXenes: A new family of two-dimensional materials. Adv Mater, 2014, 26: 992–1005
63 Lin Z, Barbara D, Taberna PL, *et al.* Capacitance of $Ti_3C_2T_x$ MXene in ionic liquid electrolyte. J Power Sources, 2016, 326: 575–579
64 Wang L, Zhang H, Wang B, *et al.* Synthesis and electrochemical performance of $Ti_3C_2T_x$ with hydrothermal process. Electron Mater Lett, 2016, 12: 702–710
65 Lei JC, Zhang X, Zhou Z. Recent advances in MXene: Preparation, properties, and applications. Front Phys, 2015, 10: 276–286
66 Li K, Jiao T, Xing R, *et al.* Fabrication of tunable hierarchical MXene@AuNPs nanocomposites constructed by self-reduction reactions with enhanced catalytic performances. Sci China Mater, 2018, 61: 728–736
67 Lin H, Chen L, Lu X, *et al.* Two-dimensional titanium carbide MXenes as efficient non-noble metal electrocatalysts for oxygen reduction reaction. Sci China Mater, 2019, 62: 662–670
68 Guo Z, Zhou J, Zhu L, *et al.* MXene: A promising photocatalyst for water splitting. J Mater Chem A, 2016, 4: 11446–11452
69 Fan Z, Wang Y, Xie Z, *et al.* Modified MXene/holey graphene films for advanced supercapacitor electrodes with superior energy storage. Adv Sci, 2018, 5: 1800750
70 Zhang Y, Zhan R, Xu Q, *et al.* Circuit board-like CoS/MXene composite with superior performance for sodium storage. Chem Eng J, 2019, 357: 220–225
71 Cheng C, Zhang X, Wang M, *et al.* Single Pd atomic catalyst on Mo_2CO_2 monolayer (MXene): Unusual activity for CO oxidation by trimolecular Eley-Rideal mechanism. Phys Chem Chem Phys, 2018, 20: 3504–3513
72 Zhang J, Zhao Y, Guo X, *et al.* Single platinum atoms immobilized on an MXene as an efficient catalyst for the hydrogen evolution reaction. Nat Catal, 2018, 1: 985–992
73 Zhao D, Chen Z, Yang W, *et al.* MXene (Ti_3C_2) vacancy-confined single-atom catalyst for efficient functionalization of CO_2. J Am Chem Soc, 2019, 141: 4086–4093
74 Chen Z, Huang S, Huang B, *et al.* Transition metal atoms implanted into MXenes (M_2CO_2) for enhanced electrocatalytic hydrogen evolution reaction. Appl Surf Sci, 2020, 509: 145319
75 Zhu J, Ha E, Zhao G, *et al.* Recent advance in MXenes: A promising 2D material for catalysis, sensor and chemical adsorption. Coord Chem Rev, 2017, 352: 306–327
76 Shen Z, Fan X, Ma S, *et al.* 3d transitional-metal single atom catalysis toward hydrogen evolution reaction on MXenes supports. Int J Hydrogen Energy, 2020, 45: 14396–14406
77 Zhang X, Zhang Z, Zhou Z. MXene-based materials for electrochemical energy storage. J Energy Chem, 2018, 27: 73–85
78 Kresse G, Furthmüller J. Efficiency of *ab-initio* total energy calculations for metals and semiconductors using a plane-wave basis set. Comput Mater Sci, 1996, 6: 15–50
79 Maniopoulou A, Davidson ERM, Grau-Crespo R, *et al.* Introducing *k*-point parallelism into VASP. Comput Phys Commun, 2012, 183: 1696–1701
80 Torrent M, Holzwarth NAW, Jollet F, *et al.* Electronic structure packages: Two implementations of the projector augmented wave (PAW) formalism. Comput Phys Commun, 2010, 181: 1862–1867
81 Torrent M, Jollet F, Bottin F, *et al.* Implementation of the projector augmented-wave method in the ABINIT code: Application to the study of iron under pressure. Comput Mater Sci, 2008, 42: 337–351
82 Jollet F, Torrent M, Holzwarth N. Generation of projector augmented-wave atomic data: A 71 element validated table in the XML format. Comput Phys Commun, 2014, 185: 1246–1254
83 Zhang Y, Yang W. Comment on "generalized gradient approximation made simple". Phys Rev Lett, 1998, 80: 890
84 Perdew JP, Burke K, Ernzerhof M. Generalized gradient approximation made simple. Phys Rev Lett, 1996, 77: 3865–3868
85 Yu M, Trinkle DR. Accurate and efficient algorithm for Bader charge integration. J Chem Phys, 2011, 134: 064111
86 Tang W, Sanville E, Henkelman G. A grid-based Bader analysis algorithm without lattice bias. J Phys-Condens Matter, 2009, 21: 084204
87 Zarkevich NA, Johnson DD. Nudged-elastic band method with two climbing images: Finding transition states in complex energy landscapes. J Chem Phys, 2015, 142: 024106
88 Henkelman G, Uberuaga BP, Jónsson H. A climbing image nudged elastic band method for finding saddle points and minimum energy paths. J Chem Phys, 2000, 113: 9901–9904
89 Kästner J, Sherwood P. Superlinearly converging dimer method for transition state search. J Chem Phys, 2008, 128: 014106
90 Henkelman G, Jónsson H. A dimer method for finding saddle points on high dimensional potential surfaces using only first derivatives. J Chem Phys, 1999, 111: 7010–7022
91 Talib SH, Yu X, Yu Q, *et al.* Non-noble metal single-atom catalysts with phosphotungstic acid (PTA) support: A theoretical study of ethylene epoxidation. Sci China Mater, 2020, 63: 1003–1014
92 Qiao B, Liang JX, Wang A, *et al.* Ultrastable single-atom gold catalysts with strong covalent metal-support interaction (CMSI). Nano Res, 2015, 8: 2913–2924
93 Wang YG, Yoon Y, Glezakou VA, *et al.* The role of reducible oxide–metal cluster charge transfer in catalytic processes: New insights on the catalytic mechanism of CO oxidation on Au/TiO_2 from *ab initio* molecular dynamics. J Am Chem Soc, 2013, 135: 10673–10683
94 Wang YG, Mei D, Glezakou VA, *et al.* Dynamic formation of single-atom catalytic active sites on ceria-supported gold nanoparticles. Nat Commun, 2015, 6: 6511
95 Tang Y, Asokan C, Xu M, *et al.* Rh single atoms on TiO_2 dynamically respond to reaction conditions by adapting their site. Nat Commun, 2019, 10: 4488
96 Chatt J, Duncanson LA. 586. Olefin co-ordination compounds. Part III. Infra-red spectra and structure: Attempted preparation of acetylene complexes. J Chem Soc, 1953: 2939–2947
97 Chatt J, Duncanson LA, Venanzi LM. Directing effects in inorganic substitution reactions. Part I. A hypothesis to explain the trans-effect. J Chem Soc, 1955: 4456–4460
98 Mao K, Li L, Zhang W, *et al.* A theoretical study of single-atom catalysis of CO oxidation using Au embedded 2D h-BN monolayer: A CO-promoted O_2 activation. Sci Rep, 2014, 4: 5441
99 Lu Z, Lv P, Xue J, *et al.* Pd_1/BN as a promising single atom catalyst of CO oxidation: A dispersion-corrected density functional theory study. RSC Adv, 2015, 5: 84381–84388

Acknowledgements This work was supported by the National Natural Science Foundation of China (21590792, 91426302, and 21433005), and Guangdong Provincial Key Laboratory of Catalysis (2020B121201002). Yu X thanks the National Science Basic Research Program of Shaanxi Province (2019JM-226). Muhammad S is grateful to the financial and

technical support from the Research Center for Advanced Materials Science (RCAMS) at King Khalid University through the Grant (RCAMS/KKU/014-20). The calculations were performed using supercomputers at Tsinghua National Laboratory for Information Science and Technology.

Author contributions Li J designed the project. Talib SH and Yu X performed the calculations. All authors discussed and interpreted the data. Talib SH, Yu X and Li J co-wrote and revised the manuscript.

Conflict of interest The authors declare no conflict of interest.

Supplementary information Computational details and supporting data are available in the online version of the paper.

Shamraiz Hussain Talib received a PhD degree at the Department of Chemistry and Key Laboratory of Organic Optoelectronics & Molecular Engineering, Tsinghua University, under the supervision of Prof. Jun Li. He received his M. Phil degree (majored in chemistry) from the Department of Chemistry, Mohi-Ud-Din Islamic University, AJ&K, Pakistan in 2016. His PhD research focuses on the theoretical investigations on heterogeneous single-atom catalysts.

Xiaohu Yu received his PhD degree from the Institute of Coal Chemistry, Chinese Academy of Sciences in 2013. He did postdoctoral research at Moscow Institute of Physics and Technology from 2013 to 2015. He worked as visiting scholar in Prof. Jun Li's group at Tsinghua University from 2019 to 2020. He is now an associate professor at Shaanxi University of Technology. His research interests focus on theoretical inorganic chemistry and computational catalysis science.

Jun Li received his PhD degree from Fujian Institute of Research on the Structure of Matter, Chinese Academy of Sciences in 1992. He did postdoctoral research at the University of Siegen and The Ohio State University from 1994 to 1997. He worked as a research scientist at The Ohio State University and a senior research scientist at the Pacific Northwest National Laboratory from 1997 to 2009. He is now a full professor at Tsinghua University. His research involves theoretical chemistry, heavy-element chemistry, and computational catalysis science.

非贵金属单原子催化剂$Co_1/MXene(Mo_2CS_2)$的CO氧化反应机理研究

Shamraiz Hussain Talib[1], Sambath Baskaran[2], 于小虎[3*], 于琦[3], Beenish Bashir[1], Shabbir Mahammad[4], Sajjad Hussain[5], 陈学年[5], 李隽[1,2*]

摘要 MXene是一类由前过渡态金属碳化物、氮化物或碳氮化物构成的新型二维材料. 我们利用量子化学方法研究了单原子Co在新型二维MXene材料Mo_2CS_2上的吸附构型、稳定性和催化性质. 研究发现Co原子可以稳定锚定在MXene材料的表面, 形成的单原子催化剂适合于催化低温CO氧化. 计算表明, 吸附的CO和O_2分子与Co_1/Mo_2CS_2催化剂表面之间的电荷转移在活化这些小分子时起着重要作用. 我们研究了Co_1/Mo_2CS_2催化氧化CO的三种机理: Eley-Rideal (ER), Langmuir-Hinshelwood (LH)和Termolecular Eley-Rideal (TER), 发现在低温下这三种反应机理都是可行的. 其中在Co_1/Mo_2CS_2催化剂上TER机理具有最高的催化活性, 计算的决速步能垒分别为0.67 (TER), 0.78 (LH)和0.88 eV (ER). 我们的研究结果表明, 利用二维材料MXene发展和设计经济的、非贵金属单原子催化剂具有重要应用前景.

